Thomas Jefferson National Accelerator Facility

JLAB-TN-01-029

UNIQUE ELECTRON POLARIMETER COMPARISON AND SPIN–BASED ENERGY MEASUREMENT

J. Grames[1]

Thomas Jefferson National Accelerator Facility,
12000 Jefferson Avenue, Newport News, VA 23606, USA

For the *Spin Dance 2000* Experiment

June 27, 2001

Abstract

A careful intercomparison of the relative analyzing power of five electron beam polarimeters was performed with the CEBAF accelerator at Thomas Jefferson National Accelerator Facility (JLab) during a dedicated two day machine development period. This is the first time such a high precision comparison between polarimeters of the Mott, Compton, and Møller type has been made. A Wien–style spin manipulator at the injector was used to vary the spin orientation of the electron beam. A series of polarization measurements as a function of spin orientation, determines the relative analyzing power between the five polarimeters. More importantly, the high statistical precision of the measurements reveal the relative differences between the polarimeters which are systematic in nature and may ultimately help realize high precision (1%) *absolute* electron polarimetry. In addition, a comparison of the value of the injector spin angle that provides precise longitudinal beam polarization at each experimental hall leads to an independent and potentially high precision absolute measurement (better than 10^{-4}) of the final electron beam energy. Results and discussion of the experiment are presented.

E-mail: grames@jlab.org
phone: (757) 269-7097
fax: (757) 269-7363

[1]This work was supported by the U.S. DOE Contract No. DE-AC05-84-ER40150.

1 Introduction

Electron beam polarimetry is the technique of separating scattered particles for detection using some physical interaction between the polarization of the beam (P) and the total analyzing power of the polarimeter's target (A_{tot}). The target is itself polarized in many polarimeter designs and A_{tot} is then proportional to the product of the target polarization and the analyzing power of the interaction. In each case the scattering process results in a measured experimental asymmetry (ϵ)

$$\epsilon = A_{tot} \cdot P. \tag{1}$$

The kinematics and design of each polarimeter determine which components of the total beam polarization are measured.

1.1 JLab Electron Beam Polarimeters

The three types of electron beam polarimeter (Mott, Compton, Møller) at Jefferson Lab are summarized in Table 1 and each is briefly described here in some detail.

Injector Mott. In order to realize a reliable and precise measurement of the beam polarization near the electron gun a high energy Mott scattering polarimeter has been developed for the injector. The Mott scattering asymmetry results from the spin–orbit coupling between the incident polarized beam electrons and the potential of the target nucleus. The polarimeter, diagnostics, and beam dump are located in the 5 MeV region of the injector and are reached by bending the electron beam -12.5° with a dipole field toward the polarimeter target. The polarimeter measures the transverse components of the beam polarization and has been studied [St99] over a range of energies ($2 - 8$ MeV) and with different high atomic number target materials (gold, silver, copper). The analyzing power (effective Sherman function) of a reference $1\,\mu$m gold target and 5 MeV beam energy used in the experiment is $S_{eff} = -0.4008 \pm 0.0014 \pm 0.0040$. The first uncertainty is instrumental and the second is the theoretical uncertainty for a zero–thickness (single atom) target used in the calibration.

Hall A Compton. Two electron beam polarimeters exist in the Hall A beamline. The first is a Compton polarimeter [Fa00], in which a Fabry-Perot optical cavity is centered in a vertical beamline chicane comprised of 4 dipoles. An external 1064 nm laser is locked to and pumps the Fabry-Perot cavity. The Compton cross–section provides a non–invasive beam measurement by scattering circularly polarized ($> 99\%$) photons which are directed at grazing angle to the incident electron beam passing through the optical cavity. The Compton backscattered photons pass through a chicane dipole and are detected using the central crystal of a 5×5 matrix of $PbWO_4$ crystals which form a calorimeter. The optical helicity can be reversed to change the overall sign of the scattering asymmetry for systematic correction. The Compton polarimeter analyzing power, which depends upon beam energy, is about 2.4% for this experiment. The combined relative uncertainty associated with the analyzing power and laser polarization amounts to 2–3%.

Hall A Møller. Downstream of the Compton polarimeter is a Møller polarimeter [Ch00] consisting of a solid polarized target, a magnetic spectrometer (3 quadrupoles and 1 dipole), and coincidence lead glass and scintillator detectors. This polarimeter uses an iron–alloy target (supermendur) which makes the measurement invasive. Either of two target foils (oriented opposing each other at small equal angles with respect to the beam direction) is polarized by a weak (240 G) longitudinal magnetic field created by a pair of Helmholtz coils. The Møller pairs (incident polarized electron and scattered target electron) are detected in coincidence. The target thickness is $\sim 13\,\mu$m, although positioned at an angle of 20° horizontally with respect to the beam, the effective target thickness is $\sim 38\,\mu$m. There is no target cooling, although

Polarimeter	*Reaction*	*Typical*	*Target*	P_{meas}
Injector Mott	$\vec{e}+ZA$	$5\,\mu$A	Gold ($1\,\mu$m)	P_x, P_y
Hall A Compton	$\vec{e}+\vec{\gamma}$	$100\,\mu$A	Photon ($\lambda = 1064\,$nm)	P_z
Hall A Møller	$\vec{e}+\vec{e}$	$2\,\mu$A	Supermendur ($10\,\mu$m)	P_z, P_x
Hall B Møller	$\vec{e}+\vec{e}$	5 nA	Permendur ($25\,\mu$m)	P_z, P_y
Hall C Møller	$\vec{e}+\vec{e}$	$2.5\,\mu$A	Iron ($4\,\mu$m)	P_z

Table 1: Summary of the five JLab electron beam polarimeters with typical current and target.

at $0.5\,\mu$A the estimated temperature increase is several degrees Kelvin and the associated relative change in target polarization is estimated to be below 0.1%; this effect is neglected in the results presented. Measurements from each of the two target foils are used to subtract the transverse analyzing power of the polarimeter.

Hall B Møller. This end station supports a Møller polarimeter [Ra00] in the Hall B beamline consisting of a solid polarized target, a magnetic spectrometer (2 quadrupoles), and coincidence detectors. This polarimeter operates at low beam currents (few nanoamps) typical of Hall B experiments. Either of two $25\,\mu$m thick permendur foils (49% Fe, 49% Co, 2% Va) are oriented vertically with their planes at $\pm 20^\circ$ with respect to the beam direction. The selected target is polarized to approximately 7.5% (along the beam direction) by a 120 G Helmholtz field. The effective analyzing power has been simulated to be $A_{zz} = -0.7826 \pm 0.0062$.

Hall C Møller. This end–station supports a Møller polarimeter [Lo96] in the Hall C beamline consisting of a solid polarized target, a magnetic spectrometer (2 quadrupoles), and coincidence lead glass and scintillator detectors. The polarimeter target is a pure iron foil positioned normal to the incident beam and within a 3 Tesla longitudinal magnetic field created by a pair of superconducting Helmholtz coils. In this target design the out–of–plane magnetization is saturated in an external field, yielding a target polarization of $\sim$ 8%. The Møller scattered electrons are detected in coincidence. The analyzing power of the polarimeter determined by Monte Carlo simulation is $A_{zz} = -0.7995 \pm 0.0060$; the uncertainty arises from the statistics of the simulation. The target polarization used is $P_z = 0.0800 \pm 0.0004$ which includes an estimate of target heating by $2.5\,\mu$A beam.

1.2 Creating the Polarized Beam

The polarized electron beam at Jefferson Lab is produced by photoemission from a semiconductor cathode using polarized laser light [Ca02, Si88, Po00]. The beam polarization depends upon critical factors which include the specific cathode material and the wavelength and degree of polarization of the incident light.

The cathode, held at a potential of $-100\,$kV, is a wafer of strained gallium arsenide activated to negative electron affinity (NEA). Irradiating the cathode with light at the wavelength of the minimum direct bandgap produces a beam of highly polarized electrons. The degree of electron polarization is directly proportional to the degree of circular polarization of the optical beam. It is straight–forward to make the optical polarization circular in excess of 99% and to expect an electron polarization greater than 70% from such a cathode. To accelerate the electrons from the cathode they must ultimately have a bunch structure compatible with the fundamental frequency (or sub–harmonic) of the accelerator RF (1.497 GHz). For a DC electron beam, characteristics of the ensemble of elec-

trons (longitudinal and transverse phase space) and components in the injection region (bunching and chopping cavities) define the fraction of electrons which are subsequently accelerated and delivered to the end–stations. Approximately 80% of a DC electron beam is lost during this process. A low efficiency use of the electron beam has a direct impact on the overall quality of the photocathode. A substantial improvement making a much more efficient use of the electrons has been made by using an RF driven diode laser [Po95] with short pulse–widths (50 ps) also synchronous with the accelerator RF (or sub–harmonic). The emitted electrons have a longitudinal profile and time–structure already compatible for high transmission through the accelerator. This improvement greatly reduces the losses of polarized beam in the chopping region.

1.3 Delivering the Beam

The accelerator, depicted in Figure 1, was configured for 5–pass recirculation and a final beam energy of 5.6 GeV. The laser source was operated in two manners, providing either a DC or RF (1497 MHz) electron beam structure. In the first case, the resulting DC electron beam was longitudinally chopped and bunched for acceleration and then delivered to the Mott polarimeter alone or to the three end–station Møller polarimeters simultaneously. The simultaneous delivery is accomplished using RF separation cavities [Ho96] which extract beam bunches in the beam switchyard to different end–stations. This mode delivered up to $\sim 4\,\mu$A per end–station. In the second mode the electron beam begins with a RF pulse structure and continues through the chopping cavities for acceleration. In this mode all beam bunches are delivered to the Hall A Compton polarimeter using a dipole magnet in the beam switchyard. As an exception, comparative measurements using the laser RF for Mott and Hall A Møller polarimeter measurements was made. The configurations are summarized in Table 2.

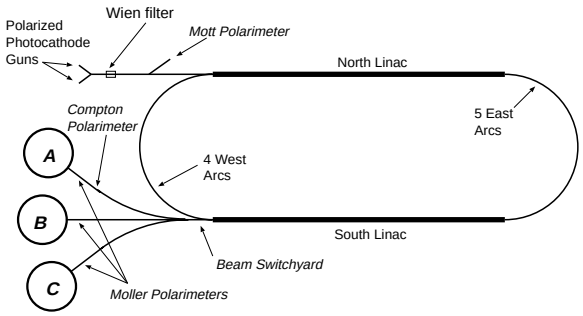

Figure 1: Schematic of the CEBAF accelerator at Jefferson Laboratory noting the Wien filter and five electron polarimeter locations.

Polarimeter	*Laser*	*Extraction*
Injector Mott	dc (rf)	D
Hall A Compton	rf	D
Hall A Møller	dc (rf)	S
Hall B Møller	dc	S
Hall C Møller	dc	S

Table 2: The polarimeters are listed with the mode of laser operation (dc=DC and rf=1497 MHz) and beam extraction (D=dipole, S=rf separator) used in the measurements.

1.4 Orienting the Beam Polarization

To precisely compare the analyzing power of the electron polarimeters criteria for orienting the beam polarization are considered. The capability for simultaneous beam delivery to multiple end–station polarimeters has the advantage that each measurement is of the same uniquely polarized beam. However, the measurable component of the beam polarization with respect to each polarimeter is generally not equal. Also, uncertainty in the total precession between the polarized electron gun and the polarimeters make a high precision measurement of the relative analyzing powers more complicated.

The solution is to perform the polarimetry in a

way which does not rely upon only one measurement of a single component of the beam polarization. This is accomplished by adjusting the orientation of the beam polarization using a spin rotator at a location common to all delivered beams. The measured components of the beam polarization can then be plotted against this orientation parameter. A fit of the data yields the experimental asymmetry and the spin rotation angle which results in the maximum longitudinal polarization at each polarimeter.

The spin rotator used to accomplish this is a Wien filter located in the injector. A Wien filter [Sa77] is a static electromagnetic device. It consists of crossed electric ($\vec{E}$) and magnetic ($\vec{B}$) fields transverse to the particle motion ($\vec{\beta}$) and each other as shown in Figure 2. The usefulness of the Wien filter is that the polarization

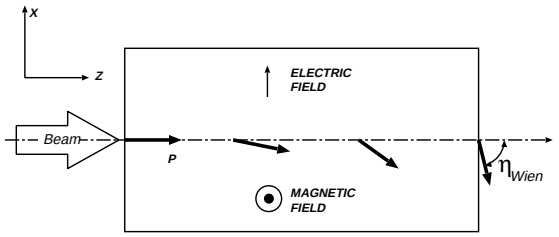

Figure 2: Diagram of Wien filter indicating the rotation of the beam polarization relative to the beam direction (η_{Wien}) in crossed magnetic and electric fields ($\beta = \frac{E}{B}$).

of a beam passing through the device can be rotated without deflecting the outgoing central orbit. This is accomplished by two conditions. First, the electric field of the Wien filter is set for the desired rotation. Second, a crossed magnetic field is applied to balance this deflecting force so that the net Lorentz force on the electron is zero

$$\vec{F} = q\left(\vec{E} + \vec{\beta} \times \vec{B}\right) = 0. \qquad (2)$$

The second condition then requires that $\beta = \frac{E}{B}$.

1.5 Concerning the Wien Angle, η_{Wien}

The Wien angle (η_{Wien}) is the spin rotation angle of the beam polarization relative to the beam momentum. It is also the independent parameter which is used to extract the amplitude and phase of the polarimeter results. The Wien angle is linear with the applied fields ($\eta_{Wien} = \eta_{\vec{E}} + \eta_{\vec{B}}$) and at the injector energy is dominated by the contribution from the electric field integral

$$\frac{\eta_{\vec{B}}}{\eta_{\vec{E}}} = \frac{-a\gamma}{\frac{g}{2\gamma} - a\gamma} = -0.17\%, \qquad (3)$$

where the Lorentz parameter $\gamma = 1.196$ at 100 keV, g is the electron gyromagnetic factor, and $a = \frac{g-2}{2} = 1.159 \times 10^{-3}$.

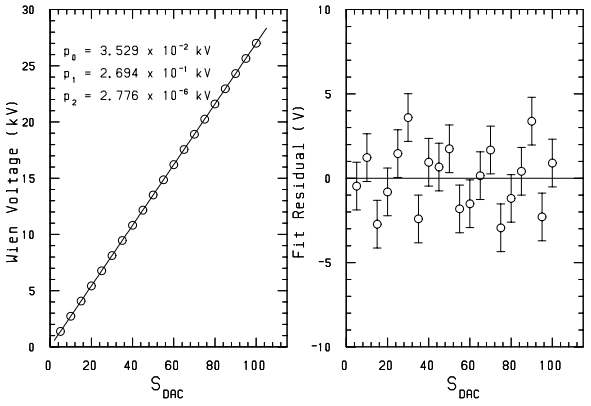

Figure 3: Differential Wien voltage with second–order polynominal fit (left) and fit residuals (right) both shown as a function of DAC setpoint (S_{DAC}). Negative voltages are achieved by reversing the polarity with a switch.

The electric field in the Wien filter is created by applying voltage to the two electrodes which span the length of the device. Since the electrodes are fixed in length the amount of spin rotation is determined by the magnitude of the differential voltage applied. Two independent power supplies controlled by a common 12–bit DAC set the electrode voltages. The 12–bit DAC is remotely set via EPICS [LANL] and is based upon a desired spin rotation angle. Note that the sign of the spin rotation is determined

by using a high voltage switchbox to switch the power supplies between the electrodes.

A calibration of power supply output was performed to determine the applied differential voltage as a function of DAC setpoint. A second–order polynominal fit of the data to account for bias voltage, gain, and linearity in response was made

$$V_{Wien} = \pm(p_0 + p_1 \cdot S_{dac} + p_2 \cdot S_{dac}^2), \qquad (4)$$

as shown in Figure 3 and reported in Table 3. The sign of the expression depends upon the state of the high voltage switchbox.

Parameter	*Value*
p_0	$(3.529 \pm 0.105) \times 10^{-2}$ kV
p_1	$(2.694 \pm 0.000) \times 10^{-1}$ kV
p_2	$(2.776 \pm 0.427) \times 10^{-6}$ kV

Table 3: Second–order polynomial fit parameter for the Wien high voltage calibration.

2 Polarimeter Measurements and Experimental Results

The entire experiment used a total of 7 eight–hour shifts. About 40% of that was spent for polarimeter checkout and debugging. The remainder of the experiment was dedicated to setting the injector (laser mode, Wien angle), the accelerator (beam extraction, energy measurement), and to polarization measurements. The pace of this portion of the experiment was quicker than expected and rather trouble-free. Polarimeter data was collected at 12 different Wien angles spanning $|\eta_{Wien}| < 110°$. The polarimeter data was analyzed by each respective polarimeter group after the experiment and is reported in Table 6.

The experimental asymmetry measured at each polarimeter is proportional to the projection of the total beam polarization along some analyzing component of the polarimeter. By performing polarization measurements at each of a series of Wien angles the component of the beam polarization which is measured at the polarimeter will vary sinusoidally with the value of the Wien angle. This dependence is modeled using the Wien high voltage calibration

$$P_{polarimeter} = P_i \cos(\lambda_i \cdot V_{Wien} + \Psi_i + \phi_g), \quad (5)$$

where P_i is the amplitude of the sinusoid and Ψ_i reflects the total spin rotation between the Wien filter and polarimeter modulo 2π. The value $\phi_g = a\gamma\theta = -0.01°$ is a correction for the 15° dipole precession between the electron gun and Wien Filter.

Polarimeter	λ_i (deg/kV)
Mott	5.553 ± 0.039
Møller A	5.664 ± 0.042
Møller B	5.694 ± 0.046
Møller C	5.611 ± 0.056
Compton	5.654 ± 0.121
Average	5.627 ± 0.022

Table 4: The best–fit results for λ_i as set by Equation 5 for the five polarimeters.

The value of λ_i is the experimentally determined coefficient which represents the scale factor between the applied Wien high voltage and spin rotation. This parameter is expected to be a constant of the experiment, however, extracting the correct value has proven difficult. Analysis of the polarimeter data indicates that λ_i varies by as much as 2.5% of itself between different polarimeter data sets. The average value of λ was calculated (see Table 4) in order to analyze the data with a unique value. The data, fit, and residuals using the average value of λ are plotted in Figure 4. The numerical results for P_i and Ψ_i are listed in Table 5.

It is important to note that the systematic uncertainties of the polarimeters are not presented

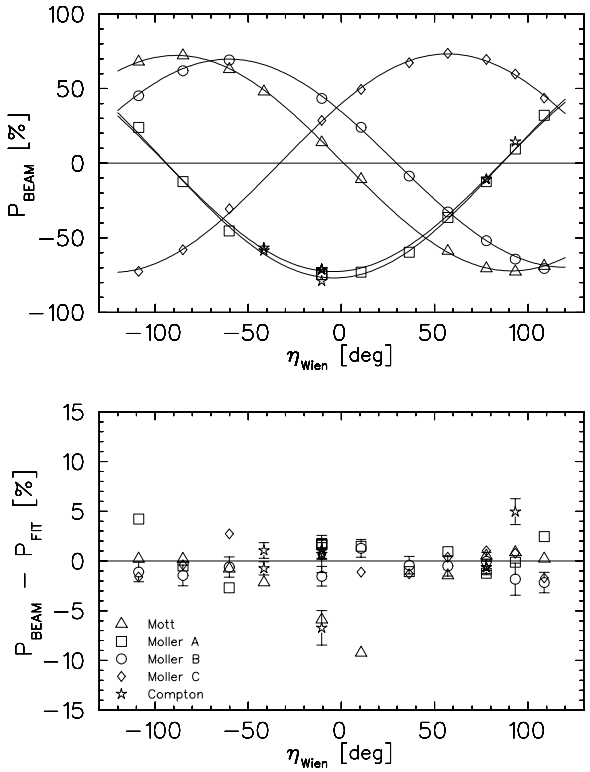

Figure 4: Polarimeter data and fit (*upper plot*) using $\lambda = 5.627°/kV$ and polarimeter statistical uncertainties only. The residuals (*lower plot*) are shown with respective statistical uncertainty.

Polar.	*Amplitude* (%)	*Phase* (*deg*)
Mott	72.21 ± 0.24	88.79 ± 0.34
	72.32 ± 0.21	*88.84 ± 0.29*
Møller-A	76.92 ± 1.11	-176.12 ± 0.62
	76.92 ± 1.12	*−176.28 ± 0.65*
Møller-B	69.71 ± 0.63	60.41 ± 0.51
	69.71 ± 0.59	*60.24 ± 0.48*
Møller-C	73.24 ± 0.54	-56.95 ± 0.63
	73.24 ± 0.57	*−56.94 ± 0.67*
Compton	72.67 ± 1.01	-175.79 ± 0.75
	72.92 ± 1.55	*−176.10 ± 1.56*

Table 5: Amplitude and phase results for polarimeter data using $\lambda = 5.627°/kV$; italicized text show the values obtained using individual λ_i. The uncertainties are total standard error in the fit parameters using a least squares fitting routine.

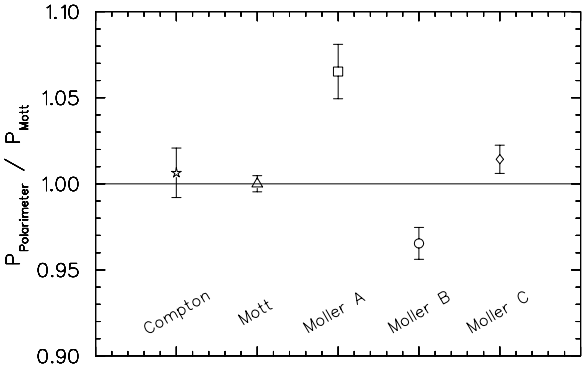

Figure 5: The relative analyzing powers for the five JLab electron beam polarimeters, normalized to the Mott polarimeter for comparison, is shown.

in these results. A motivation for this experiment is to indicate what these systematic uncertainties are by making a comparison between devices which all intend to measure the same polarized beam. A comparison of the relative analyzing powers of the polarimeters is made in Figure 5 by plotting the measured polarimeter amplitudes (P_i) with respect to a reference. In this case, the Mott polarimeter was chosen as the reference because it had the smallest relative fit uncertainty.

3 Beam Energy Measurement

The final beam energy at the polarimeters was measured by three independent methods in this experiment. The first two are spin–based and depend upon the *net* precession within the accelerator which have two main contributors; (1) precession associated to the recirculation arcs which follow successively after each linac and (2) precession associated to the transport arcs following the accelerator which deliver the beam to the end–stations. The third and independent method uses the Hall A transport arc as a magnetic spectrometer.

η_{Wien} (deg)	$Mott$ (%)	$Compton$ (%)	$M\text{ø}ller - A$ (%)	$M\text{ø}ller - B$ (%)	$M\text{ø}ller - C$ (%)
-10.54		$\mathbf{-71.05 \pm 0.90}$ $\mathbf{-71.22 \pm 0.85}$	-74.65 ± 0.17 $\mathbf{-72.33 \pm 0.14}$		
57.07	-58.90 ± 0.30		-36.42 ± 0.18	-32.65 ± 1.02	73.62 ± 0.17
108.79	-69.00 ± 0.30		$+32.09 \pm 0.14$	-70.64 ± 1.02	43.56 ± 0.26
93.27	-72.80 ± 0.30	$\mathbf{+14.41 \pm 1.30}$	$+9.45 \pm 0.10$ $\mathbf{+8.29 \pm 0.17}$	-64.31 ± 1.61	59.80 ± 0.27
77.75	-70.60 ± 0.30	$\mathbf{-10.82 \pm 0.61}$ $\mathbf{-10.81 \pm 0.74}$	-12.44 ± 0.16	-51.97 ± 0.91	69.50 ± 0.18
36.38			-59.77 ± 0.16	-8.65 ± 0.88	67.27 ± 0.18
10.54	-10.70 ± 0.40		-73.02 ± 0.14	24.05 ± 0.89	49.37 ± 0.20
-10.54	13.90 ± 0.40	$\mathbf{-71.52 \pm 1.87}$ $\mathbf{-78.95 \pm 1.73}$	-74.73 ± 0.14 $\mathbf{-73.39 \pm 0.12}$	43.40 ± 0.99	28.65 ± 0.26
-41.55	48.00 ± 0.40	$\mathbf{-58.52 \pm 0.66}$ $\mathbf{-56.71 \pm 0.79}$			
-60.16	62.90 ± 0.40		-45.38 ± 0.13	69.11 ± 1.02	-30.66 ± 0.26
-84.99	72.20 ± 0.20		-12.39 ± 0.17	61.95 ± 1.05	-58.06 ± 0.22
-108.79	68.00 ± 0.50		$+24.02 \pm 0.14$	45.19 ± 0.99	-72.59 ± 0.23

Table 6: Tabular summary of reported polarimeter measurements. Entries are for DC laser mode unless boldfaced (RF laser mode). Uncertainties are statistical only. All values use the quoted analyzing power of each polarimeter.

3.1 Method 1: Total Spin Precession

Measurement of the beam energy can be directly extracted from the total precession of the beam polarization in the accelerator. As the electron beam successively gains energy in linac sections and passes through the recirculation and end–station transport arc magnets the polarization precesses about the magnetic fields it encounters. The net polarization precession between the electron source and either of the experimental end–stations for n passes of the accelerator can be summed and written explicitly, after some algebraic manipulation, as

$$\begin{aligned}\Psi_n &= \frac{g-2}{2m_e}[(n\theta_1+(n-1)\theta_2)E_0 \\ &\quad +\frac{n}{2}((n+1)\theta_1+(n-1)\theta_2)E_1 \\ &\quad +\frac{n(n-1)}{2}(\theta_1+\theta_2)E_2 \\ &\quad +(E_0+n(E_1+E_2)\theta_h)], \end{aligned} \quad (6)$$

where E_0, E_1, and E_2 are the energy gains of the injector, north linac, and south linac, θ_1 and θ_2 are the bend angles of the east and west recirculation arcs, and $\theta_h (h \in A, B, C)$ is the bend angle of the respective end–station transport arc. By making the following transformations

$$\begin{aligned} E &= E_0 + n(E_1+E_2) \\ E_{12} &= E_1 - E_2 \\ \theta_t &= n\theta_1 + (n-1)\theta_2 + \theta_h \\ \theta_{12} &= \theta_1 - \theta_2, \end{aligned} \quad (7)$$

the total precession between the injector and an experimental hall is written in terms of model parameters which are sensible for describing the accelerator configuration. For example, it is useful to speak of the total beam energy, E, the imbalance in the linac energies, E_{12}, or the difference in the recirculation arc transport bend angles, θ_{12}. Finally, the total polarization precession through the accelerator from the injec-

tor to an experimental hall is written as

$$\Psi_n = \frac{g-2}{2m_e}[E_0\left(\frac{\theta_t-\theta_h}{2}\right)+E\left(\frac{\theta_t+\theta_h}{2}\right)+\frac{nE_{12}}{2(2n-1)}\left(\theta_t-\theta_h+(n-1)\theta_{12}\right)]. \quad (8)$$

Measurement of the total spin precession of the beam polarization in the accelerator then gives the beam energy

$$E=\frac{\frac{4m_e\Psi}{g-2}-E_0(\theta_t-\theta_h)-\frac{nE_{12}[\theta_t-\theta_h+(n-1)\theta_{12}]}{(2n-1)}}{\theta_t+\theta_h}. \quad (9)$$

The main advantage of this method is that at the maximum Jefferson Lab energies one can take advantage of the very large total precession ($\sim 10^{4\circ}$) and reach a relative measurement of the final beam energy better than 10^{-4}. The contributing uncertainties which must be minimized to achieve this are described here:

Spin Phase Advance, (Ψ). This is the measured precession between the injector Mott and an end–station polarimeter. The phase uncertainty, $\delta\Psi$, is determined from the individual fit parameter uncertainties obtained using a sinusoid fit of the polarimeter data versus Wien angle.

Injector Energy, (E_0). The injector beam energy gain can be a large contribution to the total uncertainty because it applies itself to each bend in the accelerator. The beam energy was measured prior to the experiment using the recent calibration of the injector spectrometer energy measurement [Ka99]. The beam momentum was measured absolutely to be $p = 62.89 \pm 0.1\%\,\mathrm{MeV/c}$. The corresponding injector beam energy is $E_0 = 62.89 \pm 0.06\,\mathrm{MeV}$.

Accelerator Bend Angles, ($\theta_1, \theta_2, \theta_h$). The precision to which the bend angle of the recirculation and end–station transport arcs are known also impacts the energy measurement. An extensive series of survey measurements (using a gyrotheodolite method) were performed and then compared to the original laboratory site survey grid [Cu00]. The extent to which the north and south linacs are unparallel has been determined to better than 5 arc–seconds (0.0014 degrees). The beamlines on which the Hall A and Hall C polarimeters are located were also surveyed and measured with respect to the south linac. A summary of measured and calculated bend angles used in the analysis is given in Table 7.

Survey	*Angle(deg)*
$\theta_{h=A}$	$+37.4908 \pm 0.0009$
$\theta_{h=B}$	$+0.0000 \pm 0.0100$
$\theta_{h=C}$	-37.4779 ± 0.0046
θ_1	$+180.0899 \pm 0.0014$
θ_2	$+179.9101 \pm 0.0014$
Calculated	*Angle(deg)*
θ_{12}	$+0.1798 \pm 0.0020$
$\theta_{t=A}$	$+1657.5807 \pm 0.0043$
$\theta_{t=B}$	$+1620.0899 \pm 0.0108$
$\theta_{t=C}$	$+1582.6120 \pm 0.0062$

Table 7: Summary of accelerator bend angles and uncertainties extracted from gyrotheodolite survey measurements (*upper*) and quantities calculated from those values (*lower*).

Linac Energy Gain Imbalance, (E_{12}). The polarization precession depends upon how the energy gain per pass is divided between the two linacs. Consider the case where the energy per pass is fixed. Since the west recirculation arcs always follow a full pass of the accelerator the precession there does not depend upon the equality of the linac gradients. However, the east recirculation arcs are located between the two linacs for any given pass. Consequently, the precession in the east recirculation arcs will relatively increase when $E_{12} > 0$ or decrease when $E_{12} < 0$. Unfortunately, a test to measure the linac imbalance was not performed during the two day development period. However, a benchmark test was performed a few weeks later when both linac gradients had been increased by 7%. In this case single pass beam was delivered to Hall A first using both linacs and then using only the north linac. The final beam energies

Measured	*Energy(MeV)*
E_0	67.8
$E_0 + E_1$	671.14
$E_0 + E_1 + E_2$	1270.26
Calculated	*Energy(MeV)*
E_1	603.34
E_2	599.12

Table 8: Summary of half–pass and one–pass beam delivery through Hall A arc.

extracted from the Hall A arc dipole setpoints are reported in Table 8. By comparing these and accounting for the injector energy (measurement) the linac imbalance was measured to be $E_{12} = +4.22\,\mathrm{MeV}$.

The uncertainty in the measured beam energy depends upon the component uncertainties of Equation 9 and are listed explicitly in Table 9. Finally, the final beam energy is calculated

	Expression of Uncertainty
$\frac{\partial E}{\partial \Psi}$	$\frac{4m_e}{g-2} \cdot \frac{1}{\theta_t+\theta_h}$
$\frac{\partial E}{\partial E_0}$	$-\frac{\theta_t-\theta_h}{\theta_t+\theta_h}$
$\frac{\partial E}{\partial \theta_{12}}$	$-\frac{n(n-1)E_{12}}{2n-1} \cdot \frac{1}{\theta_t+\theta_h}$
$\frac{\partial E}{\partial E_{12}}$	$-\frac{n}{2n-1}[\theta_t - \theta_h + (n-1)\theta_{12}] \cdot \frac{1}{\theta_t+\theta_h}$
$\frac{\partial E}{\partial \theta_t}$	$[-E - E_0 - \frac{nE_{12}}{2n-1}] \cdot \frac{1}{\theta_t+\theta_h}$
$\frac{\partial E}{\partial \theta_h}$	$[-E + E_0 + \frac{nE_{12}}{2n-1}] \cdot \frac{1}{\theta_t+\theta_h}$

Table 9: Relative contributions of the accelerator parameters to the total beam energy uncertainty.

from the precession between the Mott and end–station polarimeters. Results are shown in Figure 6 as a function of possible linac imbalance over the range $|E_{12}| < 20\,\mathrm{MeV}$ (1.8% imbalance).

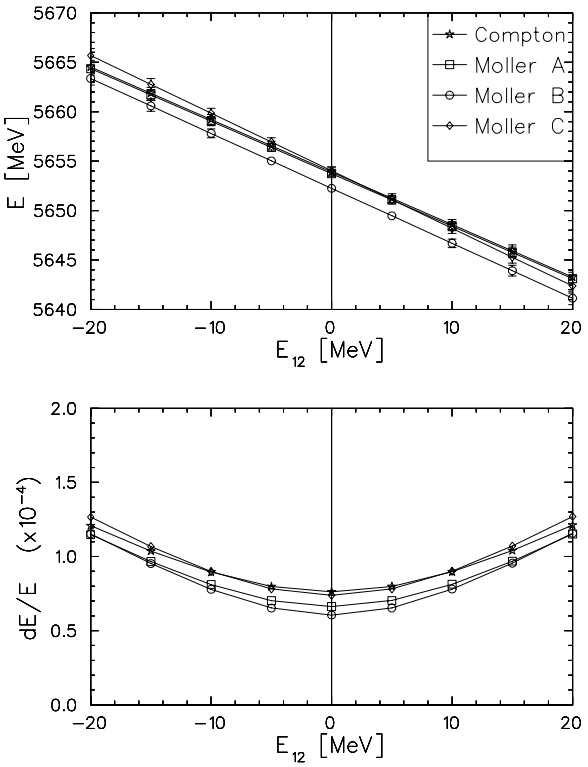

Figure 6: E and $\frac{dE}{E}$ for $|E_{12}| < 20\,\mathrm{MeV}$.

3.2 Method 2: End–Station Spin Precession

The second method compares the part of the total precession which results only from separating the beams to different end–station polarimeters following the accelerator. The advantage is that the uncertainties in the injector energy, linac imbalance, and recirculation arc bend angles are eliminated. The precession between any two end–station polarimeters is simply given by

$$\Delta\Psi = \frac{g-2}{2}\frac{E}{m_e c^2} \cdot \Delta\Theta, \qquad (10)$$

where $\Delta\Psi$ and $\Delta\Theta$ are the measured precession and bend angle between two respective end–station polarimeters. E is the final beam energy common to both. In this case the uncertainty in the bend angle is the main contribution. The disadvantage of this method is that the precession between end–station polarimeters is much smaller than that of the entire accelerator. Even at the maximum Jefferson Lab energies the relative energy measurement is $\sim 10^{-3}$. The beam

$Polarimeters(deg)$	$\Delta\Psi(deg)$	$\Delta\Theta(deg)$	$E(MeV)$	$\frac{dE}{E}$
Møller A – Møller B	483.47 ± 0.80	$+37.4908 \pm 0.0100$	5685.67 ± 9.53	1.68×10^{-3}
Møller A – Møller C	960.83 ± 0.88	$+74.9687 \pm 0.0046$	5650.71 ± 5.19	9.18×10^{-4}
Compton – Møller B	483.80 ± 0.91	$+37.4908 \pm 0.0100$	5689.55 ± 10.81	1.90×10^{-3}
Compton – Møller C	961.16 ± 0.98	$+74.9687 \pm 0.0046$	5652.65 ± 5.77	1.02×10^{-3}
Møller B – Møller C	477.36 ± 0.81	$+37.4779 \pm 0.0110$	5615.75 ± 9.67	1.72×10^{-3}

Table 10: Summary of energy measurement results comparing only end–station polarimeters.

energies extracted by intercomparing the four end–station polarimeters are given in Table 10.

3.3 Method 3: End–station A Spectrometer Method

A third comparative method, uses the Hall A transport arc as a spectrometer to determine the beam energy [Be99] to high precision. Two pairs of beam profile monitors (superharps) measure the beam direction before and after a string of 8 calibrated arc dipole magnets. The result from this measurement indicates the total 5–pass beam energy was $E = 5646.5 \pm 3.0\,\mathrm{MeV}$.

3.4 Summary of Energy Measurements

A graphical summary of the ten energy measurements is given in Figure 7. Altogether the results predict a final beam energy near 5648 MeV with variation less than 1.3%. However, the results which only compare end station polarimeters may indicate a discrepancy associated with the Hall B Møller measurements. The discrepancy is $\sim \pm 35\,\mathrm{MeV}$ ($\pm 0.6\%$) and the sign is correlated with whether the second polarimeter is located in end–station A or C. For example, a systematic shift of either (a) the Hall B precession phase Ψ by -2.9° or (b) the Hall B polarimeter orientation with respect to the other polarimeters by -0.22° could explain the discrepancy.

Excluding these three measurements the seven remaining results (total precession, end–station precession, arc spectrometer method) agree with variation $< 0.4\%$ (for $|E_{12}| < 10\,\mathrm{MeV}$). Best agreement for these measurements occur in the region of linac imbalance where E_{12} is (10 ± 2) MeV. Comparatively, the linac imbalance measured after the energy increase indicated $E_{12} = 4.2$ MeV. Note that the relative uncertainty by the total precession method in this range of E_{12} corresponds to $\frac{dE}{E} < 10^{-4}$.

4 Conclusions

A careful intercomparison of the relative analyzing powers of the five Jefferson Lab electron polarimeters of three types (Mott, Compton, Møller) was performed during a two day laboratory development period. A Wien–style spin manipulator at the injector was used to vary the spin orientation of the electron beam. A series of measurements as a function of spin orientation determine with high precision the relative analyzing powers of the polarimeters. A comparison of the Wien angle which provides longitudinal beam polarization at each polarimeter leads to a potentially high precession absolute energy measurement better than 10^{-4} of the final beam energy. Important results of the experiment are presented.

Polarimeters. It is clear from results of the relative analyzing powers that the polarimeters do not all agree on the measured beam polarization, even at the few percent level. The differences and similarities may hopefully help

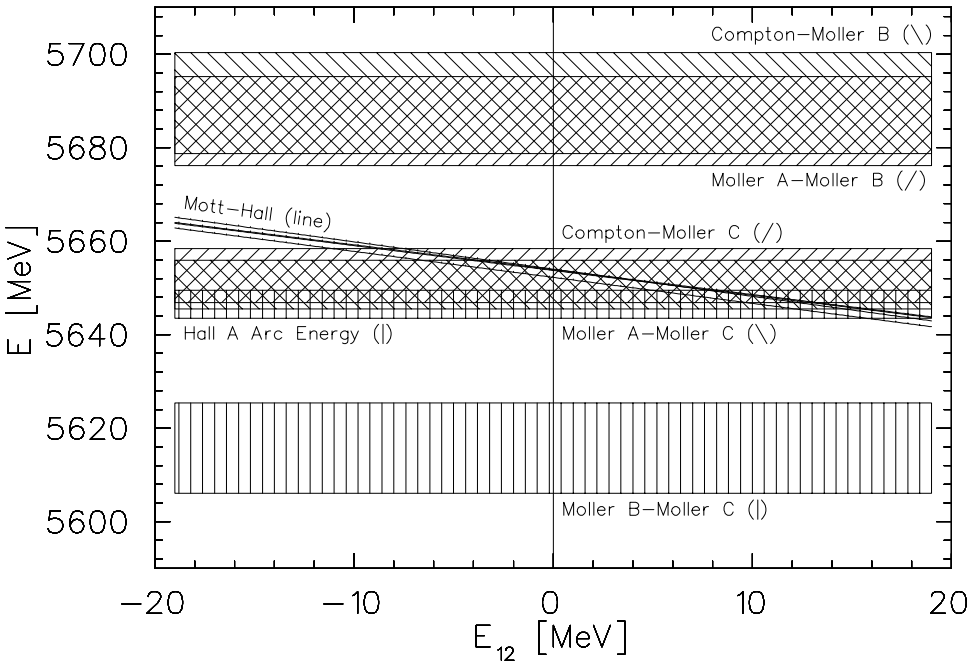

Figure 7: Graphical summary for all ten energy measurements in the range $|E_{12}| < 20\,\mathrm{MeV}$. Results which do not depend upon the linac imbalance are shown hatched and have constant bands of uncertainty. The lines which vary with E_{12} are taken from the upper plot in Figure 6.

identify how to understand the systematic effects, which may eventually lead to high precision absolute electron polarimetry. However, it is worthwhile to consider trends in the results. For example, there exists a nearly 10% disagreement between the three Møller polarimeters (all DC) while at the same time there is $< 2\%$ disagreement between a Compton (RF), Mott (DC), and a Møller (DC) polarimeter. In this case the latter two claim total systematic uncertainty better than 1.5%.

DC versus RF. There remains, in some cases, a difference between the measured polarization when either the DC or RF laser mode is used. Measurements at two greatly separated Wien angles by the Hall A Møller indicate the measured RF mode polarization is reduced. In this case the reductions are 2–3% and 12% when the beam polarization was nearly longitudinal and transverse, respectively. Yet, it is worthwhile to note that the relative analyzing powers of the Compton (RF), Mott (DC), and Hall C Møller (DC) are quite comparable. A dedicated experiment, possibly with the Mott or combination of end–station polarimeters, appears as a necessary step because of the overall implications if a DC/RF effect exists in the beam quality.

Wien filter. Calibrating the Wien angle coefficient λ reveals a few percent variation depending upon which polarimeter is considered (statistical uncertainties only). It is clear, though, that this device needs to be better characterized if absolute beam polarization uncertainties at the 1% level are to be sought by this method. The injector Mott polarimeter, which is the most sensible choice for the calibration, indicated a variation in λ by about 1% between two sets of data taken 1 month apart. In general, careful measurement of the gap high voltage and magnet current during the polarimeter data collection is certainly necessary. Operationally the beam orbit is often changed when the Wien angle is changed, particularly as the angle becomes larger. Perhaps visiting the issue of field uniformity may help unravel the few percent relative variation in Wien angle.

Energy Measurements. The energy measurements, excluding the Hall B Møller results, yield agreement better than 0.4% (for $|E_{12}| < 10$ MeV) in seven cases by three methods. The two spin–based energy measurement methods are useful because of their differences of sensitivity (to accelerator parameters) and energy resolution. The total precession method, coupled with a measurement of the linac imbalance E_{12}, can yield an absolute uncertainty better than 10^{-4}.

Future Prospects. In conclusion, Jefferson Lab has the resources to facilitate high precision absolute beam polarimetry ($< 1\%$), a common objective for the polarimeter groups. The experiment has repaid the effort and resources it required, yet the next step builds upon the present. The methods and results presented here should be considered carefully by the accelerator and polarimeter groups for planning the next measurement, to improve the overall business of polarized beam delivery at the laboratory.

5 Acknowledgements

This work is the end product of a vast amount of effort and contribution by those dedicated to producing and measuring the polarized electron beam at Jefferson Laboratory. Both J. Mitchell and C.K. Sinclair played key roles in motivating the proposal and providing me the opportunity to organize the effort. Thanks to E. Chudakov, H. Fenker, A. Freyberger, R. Kazimi, V. Lebedev, M. Poelker, M. Steigerwald, and M. Tiefenback for providing careful consideration and advice to develop the proposal. Thanks to the laboratory scheduling committee and end station leaders for supporting the experiment and its priority. Members of the Hall A Compton (C. Cavata, S. Escoffier, F. Marie, J. Mitchell, T. Pussieux), Hall A Møller (E. Chudakov, V. Gorbenko), Hall B Møller (B. Raue, V. Dharmawardane, A. Freyberger, R. Hutchins, K. Joo, R. Nasseripour, R. Suleiman), Hall C Møller (S. Danagoulian, B. Zihlmann, M. Zeier), and Injector Mott (J. Grames, J. Hansknecht, M. Poelker, M. Steigerwald) groups provided a tremendous effort and the data upon which this report is based. A special thanks to C. Curtis and the alignment group for performing the gyrotheodolite survey measurements necessary to reach the high precision spin–based energy measurement results. Thanks also to D. Higinbotham and P. Vernin for providing the comparative Hall A arc energy measurement.

References

[Be99] J. Berthot and P. Vernin, *Beam energy measurement in Hall–A of CEBAF*, Nucl. Phys. News, **9** (1999) 412.

[Ca02] L.S. Cardman, *Polarized Electron Sources for the 1990's*, Nucl. Phys. A **546**, 317c-336c (1992).

[Ch00] E. Chudakov, *Jefferson Lab Hall A 1999 & 2000 Annual Reports*, Jefferson Lab, Newport News (USA).

[Cu00] C. Curtis, Jefferson Lab Alignment Group Data Transmittals #L625, #L634, and #L643.

[Fa00] N. Falletto, *et al.*, *Compton scattering off polarized electrons with a high finesse Fabry–Perot Cavity at JLAB.*, Nucl. Instrum. Meth. A. **459**, 412 (2001).

[Ho96] C. Hovater, *et al.*, *The CEBAF RF Separator System*, Jefferson Lab TN# 96-054 (1996).

[Ka99] R. Kazimi, internal report and communication (July, 1999).

[LANL] *Experimental and Physics Industrial Control System (EPICS)* was developed jointly by LANL, ANL, CEBAF, LBL, BNL, and DESY.

[Lo96] M. Loppacher, PhD Thesis, University of Basel, Switzerland (1996).

[Po95] M. Poelker, Appl. Phys. Lett., Volume 67, Issue 19, 2762 (1995).

[Po00] M. Poelker, *al.*, *Polarized Source Performance and Developments at Jefferson Lab*, Polarized Electron Source 2000 Workshop, Nagoya, Japan (2000).

[Ra00] R. Nasseripour, B. Raue, L. Kramer, F. Fortier, *Polarization Measurements and Systematic Studies for the Hall B Moeller Polarimeter.*, Bull. Am. Phys. Soc. 45, 91 (2000).

[Si88] C.K. Sinclair, *Report on Polarized Electron Source and Electron Polarimetry Workshop*, 8th International Symposium on High Energy Spin Physics, AIP Conference Proceedings (1988).

[Sa77] M. Salomaa and H.A. Enge, *Velocity Selector for Heavy Ion Separation*, Nuclear Instruments and Methods **145** (1977) 279-282.

[St99] M. Steigerwald, private communication (October, 1999).